Bull. Disas. Prev. Res. Inst. Kyoto Univ., Vol. 18, Part 4, No. 149, March, 1969

Flow Behaviours Near the Brink of Free Overfall

By Hiroji NAKAGAWA

(Manuscript received January, 31, 1969)

1. Introduction

It makes great contribution not only to improvement of design procedures for hydraulic structures but to establishment of distribution plan for water-resources, to elucidate the hydraulic behaviours of the flow passing over the controlling devices such as the overflow spillway.

Regarding the research of the flow over the spillway, Jaeger[1] successfully derived a head-discharge relationship on an assumption about the variation of the streamline curvatures. Iwasa[2] also analyzed two-dimensional flow passing over the round crested weirs by means of the potential flow theory on the orthogonal curvilinear co-ordinates and clarified the controlling mechanism by the method of the singular point.

As for the free overfall the boundary conditions can be determinative only at the terminal section unlike for the round crested weir, so that the flow behaviours in this case have been confirmed only by the experimental procedure, or the theoretical solution of the flow to be obtained would be restricted to the terminal section. Through the experimental study conducted by Rouse[3] and the analytical one by Jaeger[4] which are well known, the investigation of the controlling mechanism is not enough to describe exactly the actual phenomena at the fall.

Hereupon, the author tries to clarify the controlling mechnism of free overfall by one-dimensional analysis with an aid of experimental research and to develop more exact method of analysis of the flow characteristics of free overfall, based on the universal law obtained by experimental investigation.

2. Controlling characteristics of free overfall

When the principle of the energy conservation is applied to the steady flow for uniform rectangular channel, the following equation of the flow profile is obtained in terms of the Cartesian co-ordinate system,

$$\frac{dh}{dx}=-\frac{\sin\theta-\dfrac{n^2q^2}{R^{4/3}h^2}-\dfrac{q^2}{2gh^2}\dfrac{d\alpha}{dx}-h\cos\theta\dfrac{d\lambda}{dx}}{\lambda\cos\theta-\dfrac{\alpha q^2}{gh^3}} \tag{2.1}$$

where the pressure coefficient λ is given as

$$\lambda=\frac{1}{qh\cos\theta}\int\left(\frac{p}{\rho g}+z\right)u\,dz \tag{2.2}$$

and the energy coefficient α is expressed by

$$\alpha=\frac{1}{q}\int\left(\frac{v}{U}\right)^2 u\,dz \tag{2.3}$$

q is the discharge rate of the flow per unit width of the channel, v is absolute value of velocity, U is mean velocity, and u is a component of velocity in x-direction.

Eq. (2.1) is approximately applicable to the curvilinear flow near the brink since it includes a correction factor for the effect of non-hydrostatic pressure condition. Neverthless, this equation is unavailable without knowledge of

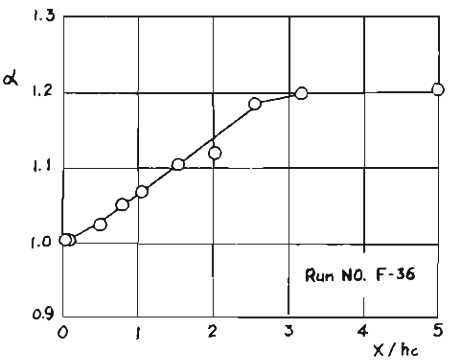

Fig. 2.1 Variation of α along the channel.

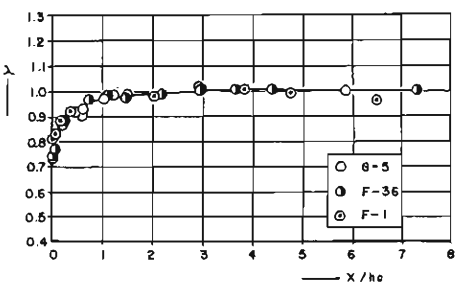

Fig. 2.2 Variation of λ along the channel.

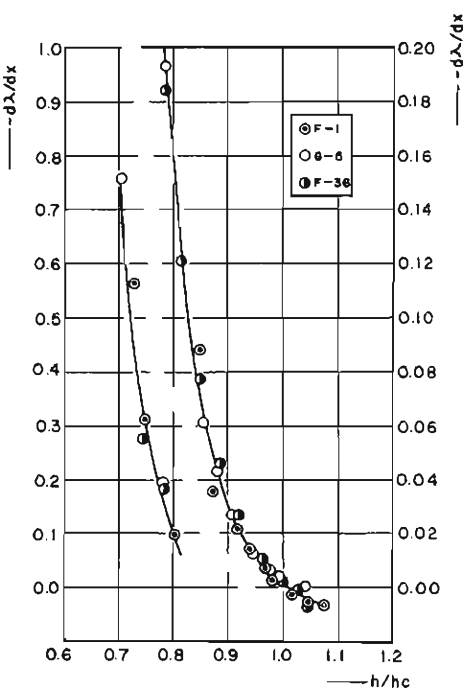

Fig. 2.3 Variation of $d\lambda/dx$ against the flow depth.

variation of the quantities α, λ, $d\alpha/dx$ and $d\lambda/dx$.

The variation of the energy coefficient α along the channel upstream from the brink is shown in Fig. 2.1. This was obtained by the velocity measurement of two-dimensional flow passing over the bottom slit with 3cm length, placed transversely at the bottom of the rectangular lucite flume. The flow upstream from the slit was proved by comparison with the results of test on free overfall to indicate as same behaviours as for the free overfall. From Fig. 2.1 it is noticed that the energy coefficient tends to approach to unity in the direction of the brink, so that $d\alpha/dx$ should be negative in the vicinity of the brink. The value of λ obtained by the pressure measurement has a tendency to decrease as the fall is approached, as shown in Fig. 2.2, in which sign

G and F designate the experiments on free overfall and bottom slit, respectively. The value of $d\lambda/dx$ obtained by substitution of the observed values of the flow depth h, α and λ in Eq. (2.1) are plotted in Fig. 2.3. It is apparent from the figure that $d\lambda/dx$ takes the negative value which rapidly decreases towards the brink.

When the flow depth is smaller than the critical depth for parallel flow $\sqrt[3]{\alpha q^2/g\cos\theta}$ as seen for the free overfall, the drop-down effect can be proved by the fact that the denominator on the right hand side of Eq. (2.1) is necessarily negative and the numerator becomes positive. The normal depth and the critical depth are given by setting the numerator and the denominator on the right hand side of Eq. (2.1) equal to zero, respectively, or

$$\sin\theta-\frac{n^2Q^2}{R^{4/3}B^2h^2}-h\cos\theta\frac{d\lambda}{dx}-\frac{Q^2}{2gB^2h^2}\frac{d\alpha}{dx}=0 \tag{2.4}$$

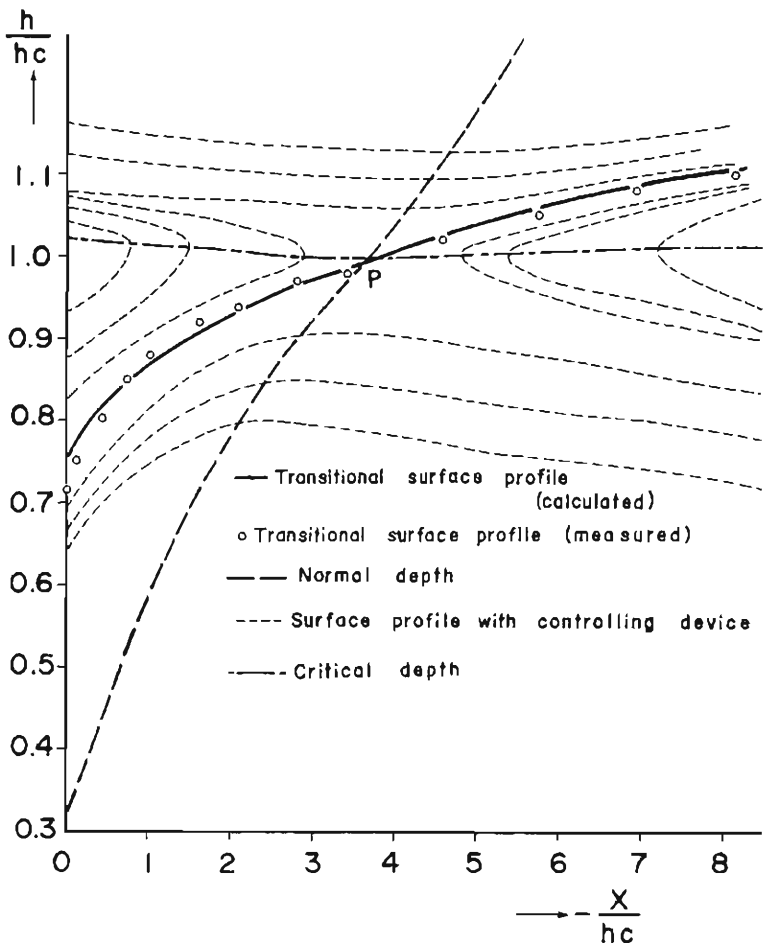

Fig. 2.4 Water surface profiles near the fall.

$$\lambda\cos\theta-\frac{\alpha Q^2}{gB^2h^3}=0 \tag{2.5}$$

The normal flow profile and the critical flow profile computed from Eq. (2.4) and (2.5) by use of α, λ, $d\alpha/dx$ and $d\lambda/dx$ given in the above figures are shown in Fig. 2.4, together with the flow profiles which are obtained by the numerical integration of Eq. (2.1) and by depth measurement. By the fact that these flow profiles intersect at a point P, it is proved that this point is a singular point, and it must be located at the section of a short distance upstream from the brink. The actual flow profile shown between the critical point and the brink does not belong to any type of flow profiles for mild bed slope designated as M1, M2 or M3 due to rapid change of the falling nappe.

Now, examine what type of flow profiles will appear around the singular point in case of the free overfall. Neglecting the variation of the velocity correction factor at the singular point, which is approved from Fig. 2.1 to be very small, and using the non-dimensional parameters refering to the flow depth at the singular point, h_c, Eq. (2.1) can be expressed as follows:

$$\frac{dh'}{dx'}=\frac{\sin\theta-\dfrac{\lambda n^2g\cos\theta}{\alpha h'^2h_c^{1/3}}\left(\dfrac{b'+2h'}{b'h'}\right)^{4/3}-h'\cos\theta\dfrac{d\lambda}{dx'}}{\lambda\cos\theta\left(1-\dfrac{1}{h'^3}\right)} \tag{2.6}$$

where, $h'=h/h_c$, $x'=x/h_c$ and $b'=B/h_c$. Transferring the origin of coordinates to the singular point and designating the new co-ordinate as (x', h'), Eq. (2.6) approximates to the following linear differential equation.

$$\frac{dh'}{dx'}=\frac{a_{21}x'+a_{22}h'}{a_{11}x'+a_{12}h'} \tag{2.7}$$

where the numerical constants a_{11}, a_{12}, a_{21} and a_{22} are given as

$$a_{11}=0,\qquad a_{12}=3\lambda_c\cos\theta,$$

$$a_{21}=-\frac{1}{\alpha_c}\left(\frac{d\lambda}{dx'}\right)_c\frac{n^2g}{h_c^{1/3}}-\cos\theta\left(1+\frac{2}{b'}\right)^{4/3}-\cos\theta\left(\frac{d^2\lambda}{dx'^2}\right)_c$$

$$a_{22}=-\frac{2\lambda_c n^2g\cos\theta}{\alpha_c h_c^{1/3}}\left(1+\frac{2}{b'}\right)^{1/3}\left(\frac{5}{3}+\frac{2}{b'}\right)-\cos\theta\left(\frac{d\lambda}{dx'}\right)_c$$

Thus, putting $k=n^2g\cos\theta\left(1+\dfrac{2}{b'}\right)^{1/3}/\alpha_c h_c^{1/3}$, the slopes of the critical flow profile and the normal flow profile at the singular point can be given by,

$$\text{Slope of the critical flow profile}=-\frac{a_{11}}{a_{12}}=0$$

$$\text{Slope of the normal flow profile}=-\frac{a_{21}}{a_{22}}=-\frac{k\left(1+\dfrac{2}{b'}\right)\left(\dfrac{d\lambda}{dx'}\right)_c+\cos\theta\left(\dfrac{d^2\lambda}{dx'^2}\right)_c}{2\lambda_c k\left(\dfrac{5}{3}+\dfrac{2}{b'}\right)-\cos\theta\left(\dfrac{d\lambda}{dx'}\right)_c}<0$$

The negative slope of the normal flow curve can be verified by the fact that $(d\lambda/dx')_c$ and $(d^2\lambda/dx'^2)_c$ become negative as shown in Fig. 2.3.

The discriminant of the characteristic equation of Eq. (2.7) ban be given as

$$D=(a_{11}+a_{22})^2-4(a_{11}a_{22}-a_{12}a_{21})$$
$$=\left\{2\lambda_c k\left(\frac{5}{3}+\frac{2}{b'}\right)-\cos\theta\left(\frac{d\lambda}{dx'}\right)_c\right\}^2$$
$$-12\lambda_c\cos^2\theta\left\{k\cos\theta\left(1+\frac{2}{b'}\right)\left(\frac{d\lambda}{dx'}\right)_c+\left(\frac{d^2\lambda}{dx'^2}\right)_c\right\}>0 \qquad (2.8)$$

And then,

$$a_{11}a_{22}-a_{12}a_{21}=3\lambda_c\cos\theta\left\{k\left(\frac{d\lambda}{dx'}\right)_c\left(1+\frac{2}{b'}\right)+\cos\theta\left(\frac{d^2\lambda}{dx'^2}\right)_c\right\}<0 \qquad (2.9)$$

From Eq. (2.9) the singular point for the free overfall becomes a saddle point which constitutes the starting point for pursuit of the flow profile.

From the above mentioned it has been ascertained that the flow depth at the fall can be determined by Eq. (2.1) and its ratio to the critical depth is dependent on the discharge rate, bed slope and roughness, as discussed later.[5]

3. Theoretical analysis of free overfall

(1) Fundamental equation for velocity distribution

The water flow under the action of gravity is expressed by the following equations of motion and continuity in vector form,

$$g\cdot\text{grad}\ H=V\times\text{curl}\ V+\nabla^2\varepsilon V \qquad (3.1)$$

$$\text{div}\ V=0 \qquad (3.2)$$

where

$$H=\frac{v^2}{2g}+\frac{p}{\rho g}+z\cos\theta+\Omega \qquad (3.3)$$

v: absolute value of the velocity, g: acceleration of gravity, p: local pressure, V: velocity vector, z: the vertical distance from the channel bottom to a point under consideration, Ω: the vertical distance from datum line to the channel bottom, and ε: the kinematic viscosity of eddy.

Using the orthogonal curvilinear co-ordinates for two-dimensional flow which consist of the s-axis along the streamline and n-axis normal from the streamline in vertical plane, Eqs. (3.1) and (3.2) are represented by

$$\frac{g}{H_1}\frac{\partial H}{\partial s}=\nabla^2\varepsilon v \qquad (3.4)$$

$$\frac{g}{H_2}\frac{\partial H}{\partial n}=\frac{v}{H_1H_2}\frac{\partial}{\partial n}(H_1v) \qquad (3.5)$$

$$\frac{1}{H_1H_2}\frac{\partial}{\partial s}(H_2v)=0 \qquad (3.6)$$

where the metrical coefficients H_1 and H_2 are given as, respectively,

$$H_1=\sqrt{\left(\frac{\partial x}{\partial s}\right)^2+\left(\frac{\partial z}{\partial s}\right)^2}$$

$$H_2=\sqrt{\left(\frac{\partial x}{\partial n}\right)^2+\left(\frac{\partial z}{\partial n}\right)^2}$$

and, H_1 and H_2 having dimension of the length, n and s should be given as non-dimensional quantities so that the value of n becomes zero at the channel bottom and unity on the free surface.

From the fact that $\partial H/\partial s$ becomes zero as confirmed later by experiment, Eq. (3.4) results in the following equation in this case.

$$\frac{g}{H_1}\frac{\partial H}{\partial s}=0$$

or

$$H=H(n) \tag{3.7}$$

Selecting a refering section in the upstream channel at which the hydrostatic distribution of pressure prevails and the velocity distribution is known, the hydraulic elements at this section are represented by

$$\left.\begin{aligned} &s=s_0\\ &H_2=h_0\\ &v=v_0(n)\\ &p=\rho g(h_0-z)\cos\theta \end{aligned}\right\} \tag{3.8}$$

The total head of the flow can be expressed by

$$H(n)=\frac{v_0^2(n)}{2g}+h_0\cos\theta+\Omega_0 \tag{3.7'}$$

As H_2v in Eq. (3.6) becomes independent on s at the refering section, the following equation can be obtained.

$$H_2v=h_0v_0(n) \tag{3.6'}$$

And Eq. (3.5) becomes

$$\frac{g}{H_2}\frac{\partial H}{\partial n}=v\left(\frac{1}{H_2}\frac{\partial v}{\partial n}+\frac{v}{H_1H_2}\frac{\partial H_1}{\partial n}\right)=\frac{v}{H_2}\frac{\partial v}{\partial n}+\frac{v^2}{R} \tag{3.5'}$$

where R is the radius of curvature of the streamline given by the following:

$$\frac{1}{R}=\frac{1}{H_1H_2}\frac{\partial H_1}{\partial n}$$

Substituting Eq. (3.7') in Eq. (3.5') and simplifying,

$$\frac{\partial}{\partial n}(v_0^2-v^2)=\frac{2H_2}{R}v^2 \tag{3.9}$$

Eq. (3.5') or Eq. (3.9) is the fundamental equation about velocity distribution for two-dimensional curvilinear flow.

Assuming that the streamline curvature can be expressed by

$$\frac{H_2}{R}=\frac{h}{R_e}n^m \tag{3.10}$$

where R_e is the radius of curvature at the water surface and m is the function of s, and, substituting Eq. (3.10) in Eq. (3.9), the linear differential

equation regarding v^2 can be obtained as

$$\frac{\partial v_0^2}{\partial n} = \frac{\partial v^2}{\partial n} + \left(\frac{2h}{R_e} n^m\right) v^2 \tag{3.11}$$

Then, the solution of Eq. (3.11) becomes

$$v^2 = \exp\left\{2\kappa(1-n^{m+1})\right\}\left\{v^2(s,1) - \int_n^1 \frac{\partial v_0^2}{\partial n} \exp(2\kappa n^{m+1})\, dn\right\} \tag{3.12}$$

where $v(s, 1)$ is the velocity at free surface ($n=1$) and

$$\kappa = \frac{h}{R_e(m+1)} \tag{3.13}$$

If the flow could be assumed to be irrotational, the velocity at a section $s=s$ can be obtained by solving Eq. (3.11) under the condition that the left hand side is equal to zero, as follow:

$$v = v(s,1) \exp \kappa\left\{1 - \left(\frac{z}{h}\right)^{m+1}\right\} \tag{3.14}$$

This is coincident with the expression for the distribution of the velocity at the fall derived by Jaeger,[6] and thus it is noticed that the integrating term on the right hand side of Eq. (3.12) represents the rotational effect of the flow.

Since the integration included in Eq. (3.12) is difficult to be solved, the problem under consideration will be discussed hereupon by approximate treatment of Eq. (3.5′). Substituting Eqs. (3.6′) and (3.7′) in Eq. (3.5′) and simplifying,

$$\frac{v_0}{v}\frac{\partial v_0}{\partial n} = \frac{\partial v}{\partial n} + \frac{h_0}{R} v_0 \tag{3.15}$$

This non-linear differential equation will be transformed into a linear form by replacing v on the left hand side of the above equation by mean velocity v_m. When the curvature of the streamlines can be represented as

$$\frac{1}{R} = \left(\frac{1}{R_e}\right) n^m, \quad m = m(s) \tag{3.16}$$

Eq. (3.15) may be reduced to

$$\frac{\partial v}{\partial n} = -\frac{h_0}{R_e} v_0 n^m + \frac{v_0}{v_m}\frac{\partial v_0}{\partial n} \tag{3.17}$$

Integrating Eq. (3.17) from $n=0$ to $n=1$, and solving for v,

$$v - v_i = -\frac{h_0}{R_e}\int_0^n v_0 n^m dn + \frac{1}{2v_m}(v_0^2 - v_{0i}^2) \tag{3.18}$$

where subscript i indicates the values at $n=0$.

(2) Velocity and pressure distributions at the brink

When the control section already described in the previous section is chosen as the refering section and the velocity distribution at this section can be given by a logarithmic form, $v_0(n)$ and $H(n)$ can be represented as, respec-

tively,

$$\left.\begin{aligned} v_0(n) &= a+b\log n \\ H(n) &= \frac{1}{2g}(a+b\log n)^2+h_c\cos\theta \end{aligned}\right\} \tag{3.19}$$

where a and b are constants to be determined by experiments and Ω included in Eq. (3.3) is disregarded hereafter due to small change of the bed level in the reach under consideration. Then, from Eq. (3.6′)

$$H_2=\frac{h_c}{v}(a+b\log n) \tag{3.20}$$

Eq. (3.18) may be transformed into

$$v-v_i=-\frac{h_c}{R_e}\left\{(a+b\log n)-\frac{b}{m+1}\right\}\frac{n^{m+1}}{m+1}+\frac{(a+b\log n)^2}{2v_m} \tag{3.21}$$

From Eqs. (3.7) and (3.19) the velocity on the upper nappe at brink, v_e, and on the lower nappe, v_i, can be given, respectively:

$$\left.\begin{aligned} v_e &= \sqrt{a^2+2g(h_c-h_r)\cos\theta} \quad (n=1) \\ v_i &= \sqrt{2gh_c\cos\theta} \quad (n=0) \end{aligned}\right\} \tag{3.22}$$

where h_r is the depth normal to the channel bed at the brink.

Though the velocity given by Fq. (3.19) may take negative value for smaller values of n, the following analysis will be made reasonably on an assumption of zero velocity for this range of n. Substituting Eq. (3.22) in Eq. (3.21) and dividing by $\sqrt{gh_c}$, the following may be written by use of the relationship $v_{mc}=a-b$ obtained from Eq. (2.19),

$$\sqrt{\eta^2+2(1-\xi)}-\sqrt{2}=-\frac{h_c(\eta m+1)}{R_e(m+1)^2}+\frac{\eta^2\xi}{2} \tag{3.23}$$

where $\eta=a/v_{mc}$, $\xi=h_r/h_c$ and v_{mc} is approximately given by $\sqrt{gh_c}$ ($h_c=\sqrt[3]{q^2/g}$).

The flow depth at the brink can be represented by the metrical coefficient H_2 as follow:

$$h_r=\int_0^1 H_2\,dn \tag{3.24}$$

Solving the above four Equations (3.20), (3.21), (3.23) and (3.24) simultaneously, the unknown v, H_2, m and R_e/h_c can be determined for given values of η and ξ.

Eliminating R_e/h_c from Eqs. (3.21) and (3.23), v can be represented as a function of m only; that is,

$$\frac{v}{v_m}=\frac{\sqrt{\eta^2+2(1-\xi)}-\sqrt{2}-(\eta^2\xi/2)}{\eta m+1}\left\{(\eta-1)(m+1)\log n+(\eta m+1)\right\}n^{m+1}$$
$$+\frac{\xi}{2}\left\{\eta+(\eta-1)\log n\right\}^2+\sqrt{2} \tag{3.25}$$

Also, from Eqs. (3.20) and (3.24),

$$\xi=\int_0^1 \frac{a+b\log n}{v}\,dn \tag{3.26}$$

From Eqs. (3.25) and (3.26), v and m can be solved.

Between n and z the following may be written:

$$z=\int_0^n \frac{h_c(a+b\log n)}{v}\,dn \tag{3.27}$$

and from this equation and Eq. (3.24) the relationship between n and z/h_r can be established.

The pressure distribution at the brink can be obtained by substituting Eqs. (3.25) and (3.27) in the following energy equation:

$$\frac{1}{2g}(a+b\log n)^2+h_c\cos\theta=\frac{v^2}{2g}+\frac{p}{\rho g}+z\cos\theta \tag{3.28}$$

4. Experimental verification to theoretical analysis of free overfall

The experiments to verify the theoretical analysis on hydraulic behaviours of the free overfall has been conducted at the Ujigawa Hydraulis Laboratory, Disaster Prevention Research Institute, Kyoto University. The apparatus employed consisted of a rectangular lucite flume 0.25 m wide, 0.20 m deep and 9,0 m long with a constant bed slope of 1/1,000 downward. The discharge rate varied from 7.5 to 2.00 liters per second. The velocity and pressure in the stream were measured by a tilting Pitot tube directed to the flow, in combination with a direction string to detect the direction of the flow at any point.

(1) Verification to assumptions on analysis

(i) The ratio of the depth at brink to the critical depth, ξ.

Fathy and Shaarawi[7] concluded by their experimental research that the value of ξ for free overfall decreased as the bed slope increased and there was a definite value of the Froude number at the brink for a given bed slope, independent of the discharge rate. The experiments on the horizontal bed conducted by the other investigators[8,9] indicated value of ξ to become 0.715 to 0.724. By authors' experiment for five kinds of discharges it has been indicated that the value of ξ is constant to be 0.711 for a bed slope of 1 in 1,000.

(ii) Velocity distribution at critical point.

The result of velocity measurement for six runs showed that the velocity distribution at the critical point was practically represented by the following:

$$\frac{v_c}{v_{mc}}=1.1+1.0\log\frac{z}{h_c}$$

(iii) Vertical distribution of energy.

Typical examples of the vertical distribution of the energy head which have been obtained by the velocity and pressure measurements are shown in Fig. 4.1. As evidently seen in the figure, it will be recognized that the values of the energy for same values of z/h are consistent for different sections on upstream side of the brink, and consequently the basic assumption for con-

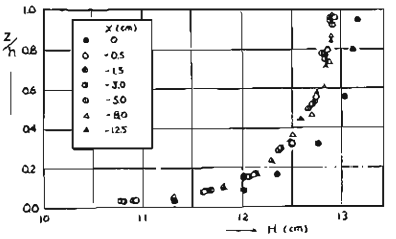

Fig. 4. 1 Vertical distribution of energy.

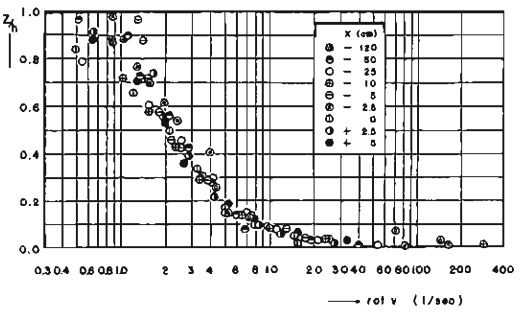

Fig. 4. 2 Vertical distribution of vorticity.

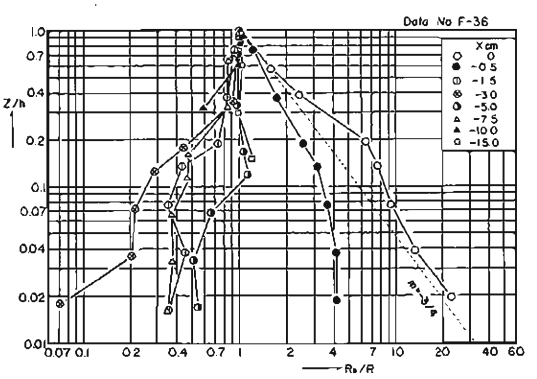

Fig. 4. 3 Vertical distribution of curvature of streamlines.

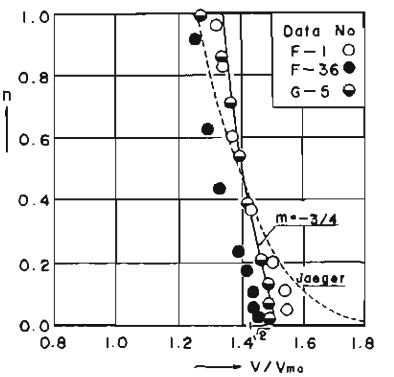

Fig. 4. 4 Velocity distribution at the brink.

stant energy along a streamline as indicated by Eq. (3. 7) is verified.

By the fact that the energy tends to decrease downward at any section it is also proved that the flow of the free overfall should be treated as the rotational flow. From Eqs. (3. 5) and (3. 6′),

$$y\text{-component of curl } V=-\frac{1}{H_1H_2}\frac{\partial}{\partial n}(H_1\cdot v)=\frac{g}{H_2v}\frac{\partial H}{\partial n}=\frac{g}{h_0v_0(n)}\frac{\partial H}{\partial n}$$

Then, since H is dependent on n only, curl V should also be dependent on n only, and consequently it is understood that vorticity will be conserved along a streamline, as apparently indicated in Fig. 4. 2 in which the vorticity distributions at different sections are plotted against z/h.

(iv) Distribution of curvature of streamlines.

Substituting the observed values of the velocity and pressure in Eq. (3. 5′) and approximating H_2 to be equal to z/h, the vertical distribution of curvature of the streamlines can be obtained as shown in Fig. 4. 3. From the figure which indicates the linear variation of the curvature at any section, it is proved that the assumption represented by Eq. (3. 16) may be satisfied.

(2) Verification to theoretical expression

As already described, the distributions of velocity and curvature at the brink

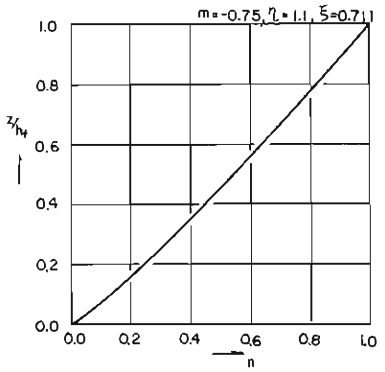

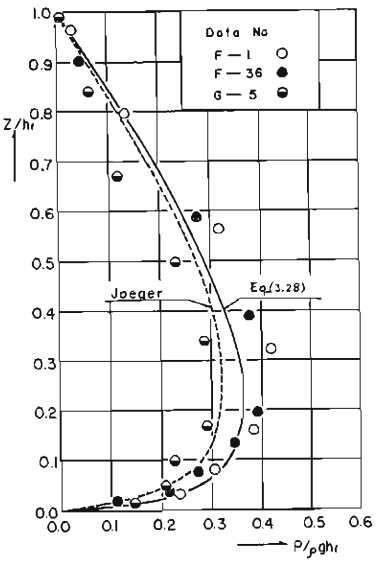

Fig. 4.5 Correlation curve between z and n. Fig. 4.6 Pressure distribution at the brink.

can be determined by solving simultaneously Eqs. (3.25) and (3.26). Using 0.711 as a value of ξ, the corresponding value of m is found to be -0.75 and this indicates a good agreement with the observed values.

The calculated curve of the velocity distribution is shown in Fig. 4.4, together with the velocity distribution pattern of the irrotational flow derived by Jaeger and observed values obtained by author's tests on the free overfall and transversal bottom slit. It is indicated that Eq. (3.25) gives a fairly good agreement with the observed values, while the solution based on an assumption of the irrotational flow shows to deviate from the measurements in the vicinity of the channel bed due to disregard of $\partial H/\partial n$ which takes a large values near the bed.

The correlation curve between z and n at the brink computed from Eq. (3.27) is shown in Fig. 4.5. This curve indicates that in the vicinity of the bed the streamlines close together more densely and so the value of H_2 has a tendency to decrease. From this indication it is concluded that on analyzing the flow of free overfall the assumption for constancy of H_2 to be equal to h_r as seen in Iwasaki's study[10] is inadequate.

The pressure distribution at the brink which is computed by use of Eq. (3.28) and z-n relationship given in Fig. 4.5 is indicated in Fig. 4.6. It will be due to unskilled measurement of pressure in the high velocity curvilinear flow that the observed pressure has shown lower value than the calculated one throughout the depth in case of the free overfall.

5. Conclusion

The flow behaviours of the free overfall have hitherto been analysed as the irrotational flow in view of simplicity of solution. The present paper is to

describe the hydraulic characteristics of the free overfall more exactly by treating it as the rotational flow as verified by the experiment. The complete description of the flow is not obtained because of great complexity to determine the boundary conditions. Neverthless, it will expected that the investigation described herein contribute to further development of the analytical procedures on the rapidly varied flow.

The conclusions obtained through this study are summarized as follows:

(1) The energy coefficient and pressure coefficient represented by one-dimensional analysis have a tendency to decrease as the brink is approached.

(2) A singular point which appears at a short distance upstream from the brink is proved to be a saddle point at which the control of flow is achieved.

(3) The theoretical expressions about hydraulic characteristics of the rotational curvilinear flow derived on the assumption for constant energy along a streamline have been verified to represent the actual phenomena at the brink with a fair accuracy.

(4) The curvature of a streamline at the brink has a tendency to increase exponentially toward the bed, while it decreases at the sections in upstream channel.

Acknowledgements

The research has been conducted by the author with cooperation of other staff and students participating to hydraulics in Ujigawa Hydraulic Laboratory, Disaster Prevention Research Institute, Kyoto University.

Deep acknowledgements of the author are made to Messrs. T. Utami and Y. Ichihashi for their hearty assistance. The author wishes to express his gratitude to the Matsunaga Science Fund. for its support of this work.

Bibliography

1) Jaeger, C.: Engineering Fluid Mechanics, Blackie, London, 1956.
2) Ishihara, T., Iwasa, Y. and Ihda, K.: Basic Studies on Hydraulic Preformances of Overflow Spillways and Diversion Weirs, Bulletin, D. P. R. I., Kyoto University, No. 33, March 1960.
3) Rouse, H.: Discharge Characteristics of the Free Overfall, Civil Engineering, Vol. 6, April 1936.
4) Jaeger, C.: Hauteur d'eau a l'extremite d'un long deversoir, La Houille Blanche, Nov.-Dec. 1948.
5) Nakagawa, H.: On Hydraulic Performance of Bottom Diversion Works, Bulletin No. 143, D. P. R. I., Kyoto University, Part III, 1969.
6) Jaeger, C.: Ibid., 4) p. 519.
7) Fathy, A. and Amin, M. S.: Hydraulics of the Free Overfall, Proc. of ASCE, Vol. 80, Sep. No. 564, Dec. 1954.
8) Rouse, H.: Ibid., 3).
9) Iwasaki, T.: An Experimental Investigation on Hydraulics of the Free Overfall Proc. of JSCE, June 1953, pp. 241-246 (in Japanese).
10) Iwasaki, T.: Ibid., 9).